Supporting Information

Rutile phase *n*- and *p*-type anodic titania nanotube arrays with square-shaped pore morphologies

Piyush Kar [1*], Yun Zhang[1], Samira Farsinezhad[1], Arash Mohammadpour[1], Benjamin D. Wiltshire[1], Himani Sharma[1], and Karthik Shankar[1, 2]*

[1]*Department of Electrical and Computer Engineering, University of Alberta, 9107 - 116 St, Edmonton, Alberta, Canada T6G2 V4*

[2]*NRC National Institute for Nanotechnology, 11421 Saskatchewan Dr. NW, Edmonton, AB T6G 2M9*

† Electronic supplementary information (ESI) available: experimental section and supplementary figures.

*** Authors to whom all correspondence must addressed:**

1. Dr. Piyush Kar, pkar1@ualberta.camailto:pxkk213@gmail.com
2. Prof. Karthik Shankar, kshankar@ualberta.camailto:kshankar@ualberta.ca

Contents

Experimental, materials and methods

An aqueous solution containing 1% (v/v) hydrofluoric acid (HF) and 8 % acetic acid (known to produce mechanically robust nanotubes), was used as the electrolyte for anodic synthesis in a two-electrode cell. Titanium foils 1 cm in width, 4 cm in length and 0.089cm in thickness were used as working electrode or anode. A cylindrically shaped graphite electrode of 0.3 cm diameter and 4 cm length was used as the cathode. The inter-electrode spacing was 3 cm and the electrolyte volume was 15 ml. Electrochemical anodization was performed at 15 V for 1 hour at room temperature. Post-anodization annealing in furnace was conducted in the presence of air for 3 hours at 450 °C - this type of sample will be referred to as low temperature annealed nanotubes (LANT) in the reminder of this report. LANTs were precursors for the other two types of nanotube samples synthesized and characterized. Flame annealed nanotubes (FANT) were generated using a Benzomatic Fatboy propane torch containing a standard pen-type nozzle, with the sample held approximately 4 cm from the tip of the nozzle, which lies within the reducing region of the flame, where the temperature was measured using a hand-held laser temperature gun and found to be approximately 650 °C. High temperature annealed nanotubes (HANTs) experienced 750 °C for two hours in air in a tube furnace. Imaging of sample morphologies was performed usingHitachiS4800 field emission scanning electron microscope (FESEM). Phase characterization was conducted by grazing incidence X-ray diffraction (GIXRD) on a Bruker D8 Discover instrument with a sealed Cu tube X-ray source and by Raman spectroscopy using a Nicolet Almega-XR Raman microscope excited by a 532 nm laser source. Transmission electron microscopy (TEM) imaging was performed by using a JEOL 2200 FS TEM at an acceleration voltage of 200 kV. Electrochemical impedance spectroscopy and Mott Schottky data were collected in a three-electrode electrochemical cell with Ag/AgCl reference electrode using a CHI

600D potentiostat (CH Instruments, Inc.). All electrochemical measurements used a 0.1 M phosphate buffer solution electrolyte at pH 7.4 and at room temperature. The photo-electrochemical properties of the three different nanotube types were investigated using a standard three-electrode electrochemical cell, where the electrolyte was 1 M KOH, reference electrode was Ag/AgCl, and counter electrode was a Pt-coated glass slide. The electrochemical measurements were conducted using the same potentiostat described above. For experiments conducted in light, we employed AM 1.5G one sun intensity using a Newport solar simulator bearing Class A filters. X-ray photoelectron spectroscopy (XPS) was conducted using an Axis Ultra spectrometer from Kratos Analytical.

An additional note about HANTs

As it can be observed in **Fig. S1.**, in certain sections, HANTs are divided into two layers. These layers are formed by variation in heat transfer rates, where faster heat transfer occurs from the section of nanotubes at the top than from those in the interior. These top nanotube layers bear L-shaped sections (likely due to thermal strains) in addition to full square shaped nanotubes. In some instances the inner layer, which is perfectly square shaped, is visible from the top view as marked by the inserted circle in **Fig. S1.** (a). When the samples are cooled at a faster rate, i.e. from 750 °C to room temperature in about three hours, the outer layer completely peels off exposing the inner layer. The inner layers exhibit a more regular square shapes and do not contain the L-shaped sections, as shown in Fig. S2. These inner layers are characterized by an average wall thickness of about 15 nm and an average wall spacing of 20 nm.

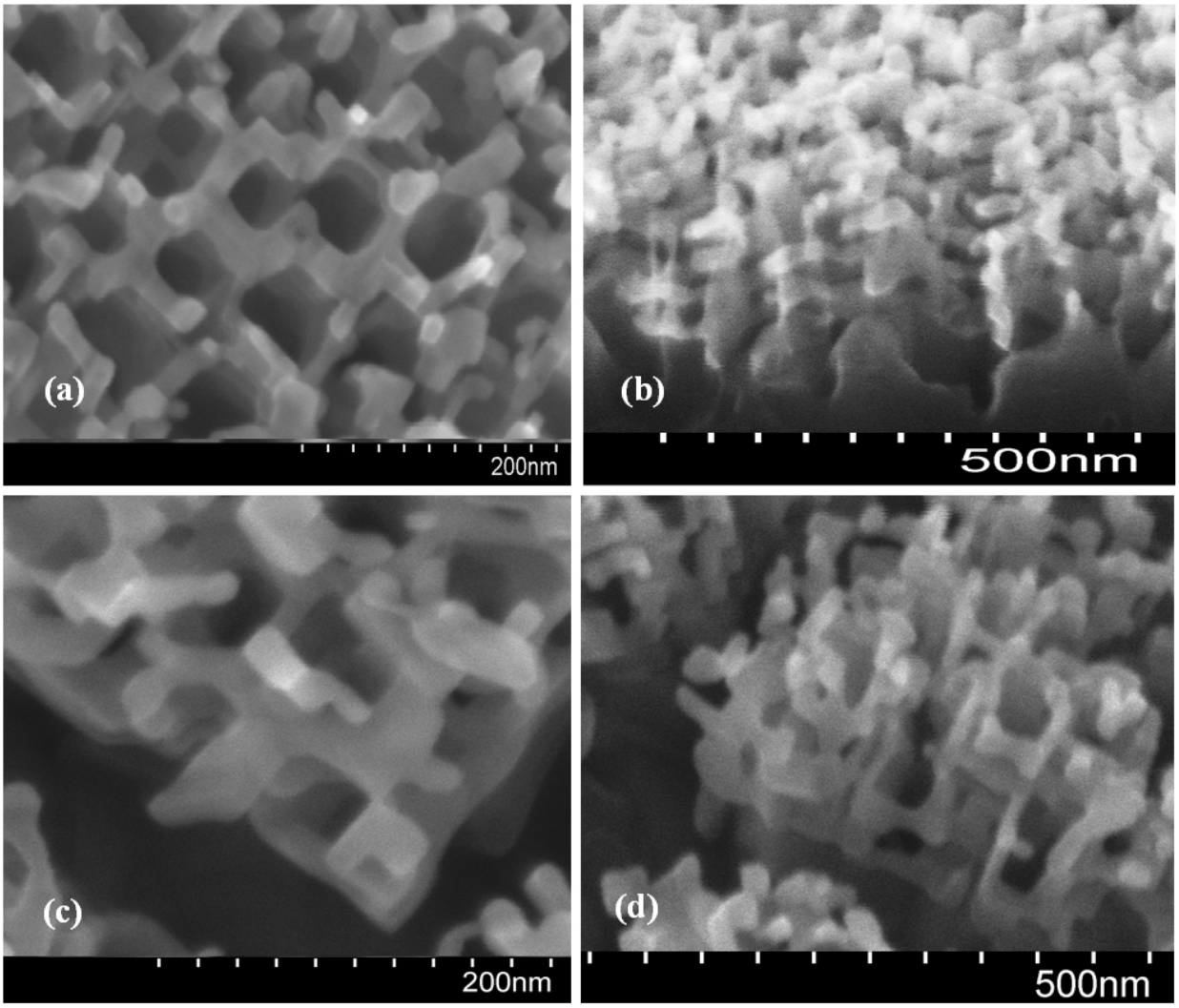

Fig. S1. Additional FESEM images, (a) and (c) are top views of HANTs, and (b) and (d) show their cross-sections.

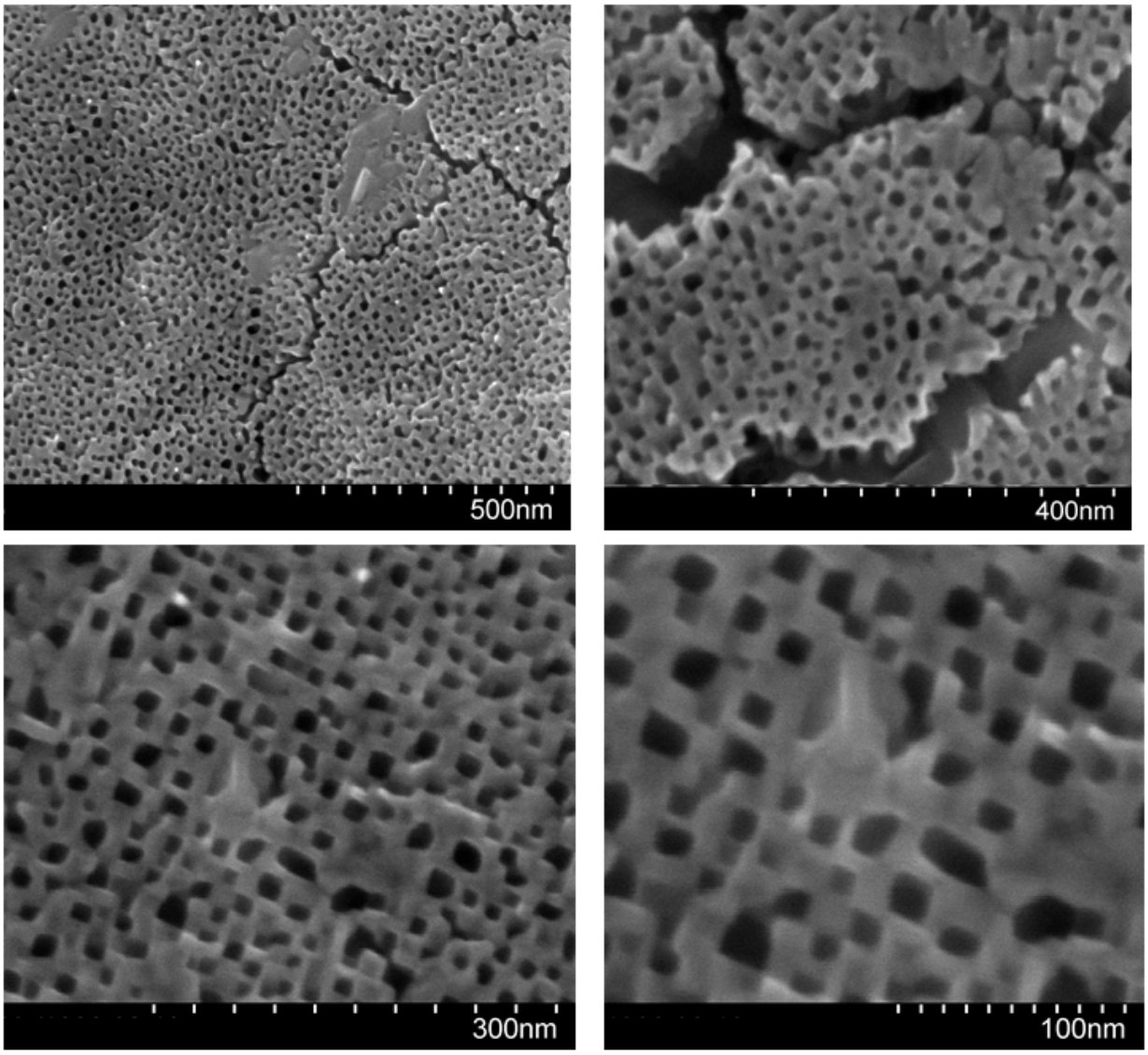

Fig. S2. Top view FESEM images of the inner nanotube layer in HANTs

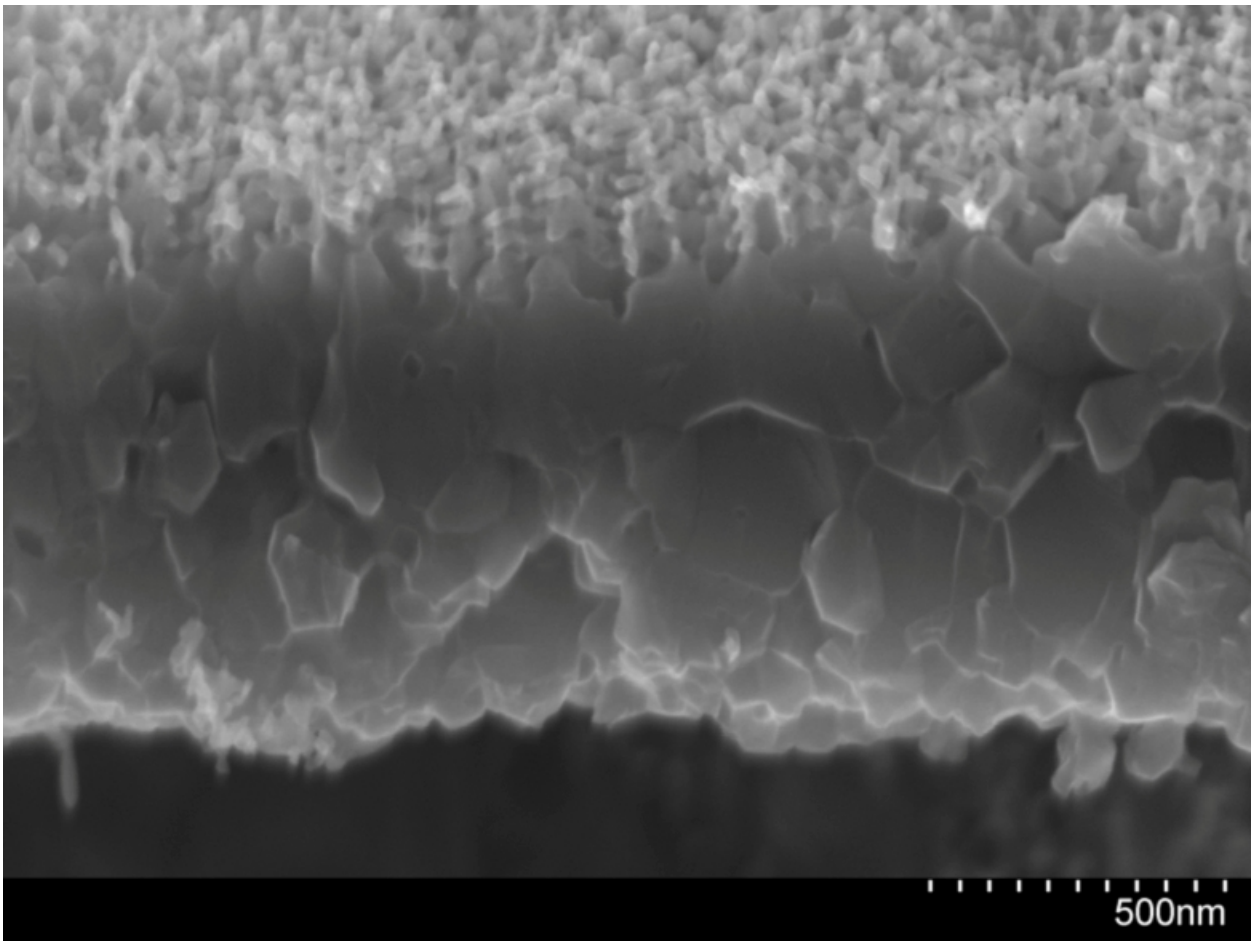

Fig. S3. FESEM image showing the full barrier layer of HANTs

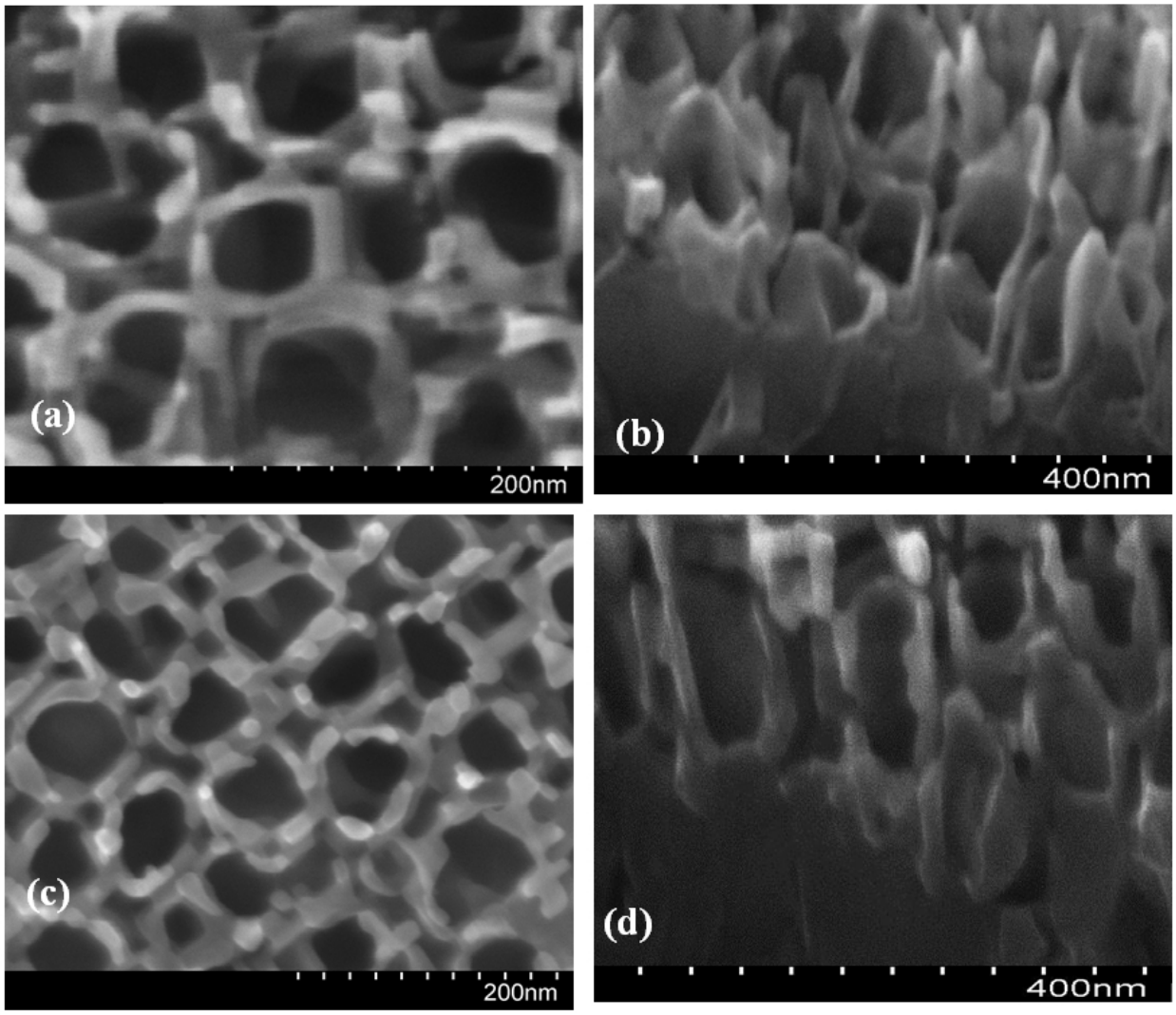

Fig. S4. Additional FESEM images, (a) and (c) are top views of FANTs, and (b) and (d) show their cross-sections.

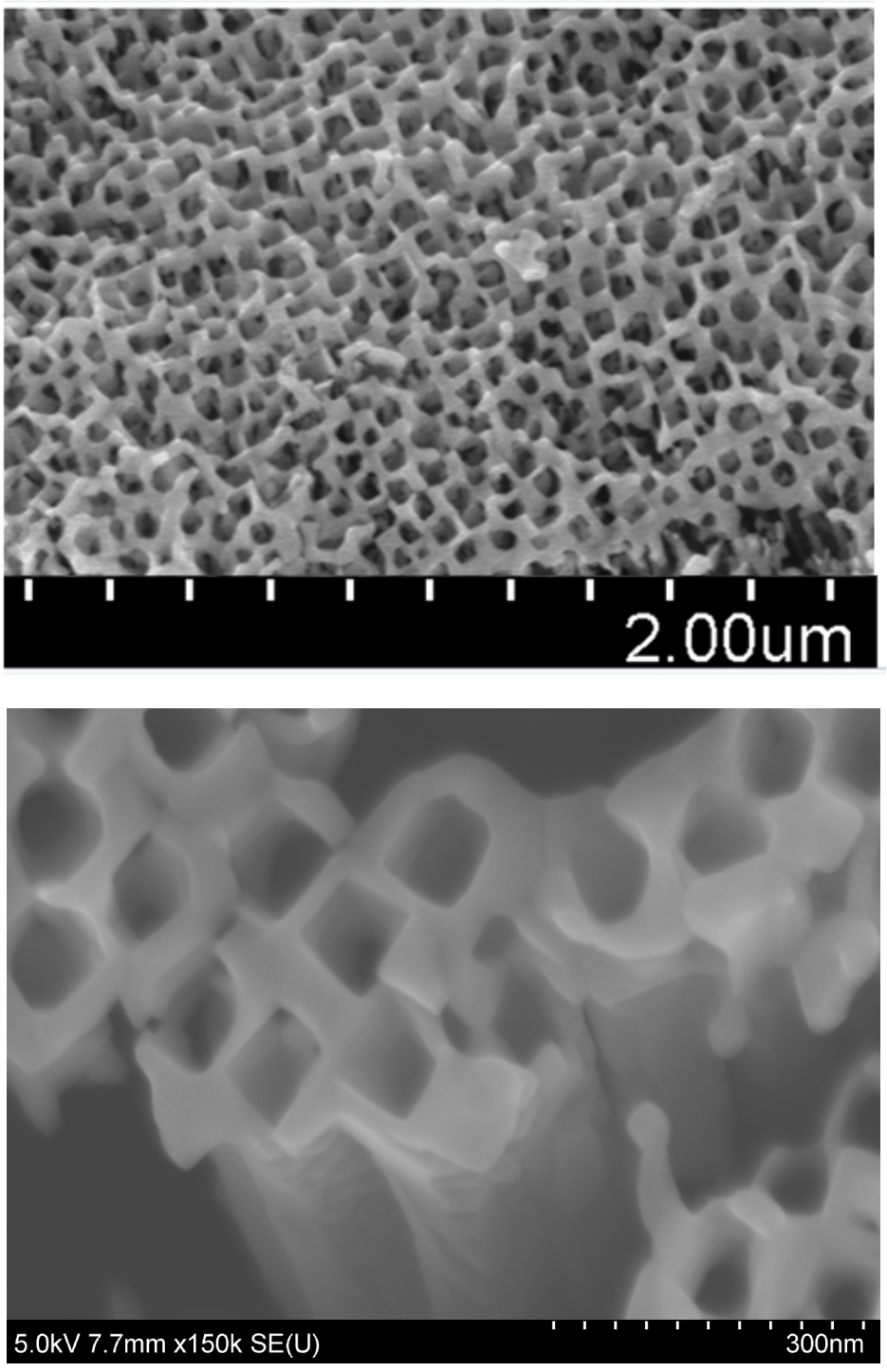

Fig. S5. Top-view and cross-sectional FESEM images of flame annealed ethylene glycol anodized TiO_2 nanotubes exhibiting square pore morphology.

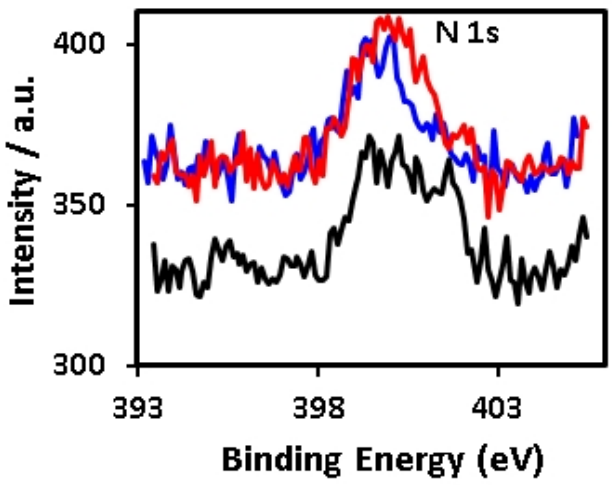

Fig. S6. N 1s XPS spectrum for the three types of nanotubes, i.e. FANTs (red), HANTs (black) and LANTs (blue).

EIS analysis

Nyquist plots of the FANTs, LANTs, and HANTs containing measured data and curve fits at different potentials (shown in **Fig. S7.** (a), (b) and (c), respectively) represent the AC electrochemical impedance behavior of the three types of nanotubes. Equivalent circuits (ECs) used for fitting the EIS data are shown in **Fig. S7**. (d)**,** for LANTs and FANTs, and in **Fig. S7.** (e)**,** for HANTs. The ECs have an electrolyte resistance element, called $\boldsymbol{R_s}$ and a constant phase element ***CPE*** (represented by $\boldsymbol{Q_2}$ and $\boldsymbol{n_2}$, or $\boldsymbol{j}$ =2) in series with time constant(s). The generic transport resistance is termed $\boldsymbol{R_t}$. A single time constant given by space charge capacitance $\boldsymbol{C_j}$ parallel to a series combination of transport resistance $\boldsymbol{R_1}$ and ***CPE*** (represented by $\boldsymbol{Q_1}$ and $\boldsymbol{n_1}$, or $\boldsymbol{j}$ =1) is applicable to the impedance spectra for the FANTs and the LANTs. Similar ECs for TiO_2 nanotube arrays are reported in other reports.[1-3] Two time constants in series, as shown in **Fig. S7**. (e), are applicable to the HANTs, where the transport resistance is $\boldsymbol{R_2}$. Capacitive impedance is given by **eq. [1]** and impedance due constant phase elements is given by **eq. [2].**

$$Z_{C_j} = \frac{1}{(i\omega)^{n_j} Q_j} \quad [1]$$

$$Z_{Q_j} = \frac{1}{(i\omega)^{n_j} Q_j} \quad [2]$$

In **[1]** and **[2]**, $i = (-1)^{0.5}$, where ω is the angular frequency given by $2\pi f$, where f is the frequency of the applied alternating current (AC) signal. The total impedance of the system, as illustrated by the EC, was calculated and fitted to experimental data to extract the circuit parameters. Between -0.5 V and -1 V (w.r.t. Ag/AgCl), the charge transport resistance R_t, which measures carrier transport from the bulk to the semiconductor-electrolyte interface, varied in the range 0.05- 10 kΩ for LANTs and FANTs **(Fig. S7.** (f)**)**. HANTs, on the other hand, exhibited R_t of the order of MΩs, which is indicative of a distinctly thicker barrier layer in HANTs. As shown in the capacitance versus potential (C-V) plot (**Fig. S7.** (g)), the capacitance of the HANTs was found to be many orders of magnitude lower than the same for FANTs and LANTs. Given the inverse relationship between capacitance and thickness, this result provides further confirmation for a much thicker barrier layer present in HANTs compared to FANTs and LANTs.

This effect of potential on transport resistance conformed to resistive behavior at higher potentials and to capacitive behavior at negative potentials for FANTs and LANTs. Variation of R_t with potential was minimal in case of the HANTs. The variation of R_t, for FANTs and LANTs matches with the variation of their ***CPE*** exponent n_2 that increased from 0.5 at 0.5 V to 0.65 at -1.0 V (w.r.t. Ag/AgCl). The physical implication of ***CPE*** exponent ≈0.5 is a semi-infinite diffusion-limited reaction of rutile film, which may be due to oxidative formation of TiO_3 at positive potentials. ***CPE*** exponents, n_1, for both LANTs and FANTs, assume capacitive

values at or near flat band potentials (reported in the next section). Resistive ***CPE*** exponents, n_1 and n_2, were obtained for HANTs.

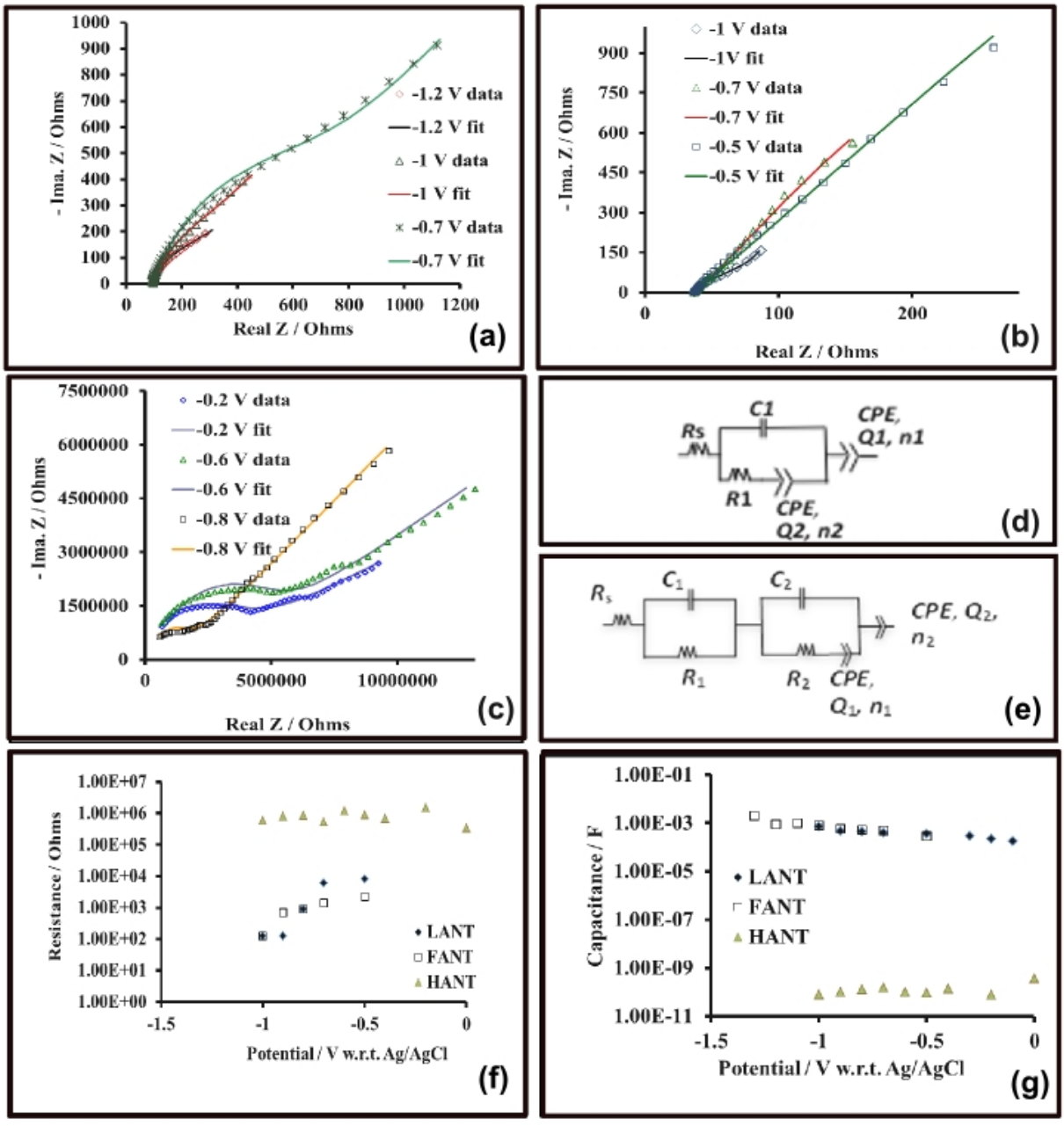

Fig. S7. (a), (b) and (c) Nyquist plots at selected potentials for FANTs, LANTs, and HANTs, respectively; (d) is the equivalent circuit for FANTs and LANTs; (e) Equivalent circuit for HANTs; (f) Plot of transport resistance versus potential for the three nanotube types; (g) Plot of capacitance versus potential for the three nanotube types.

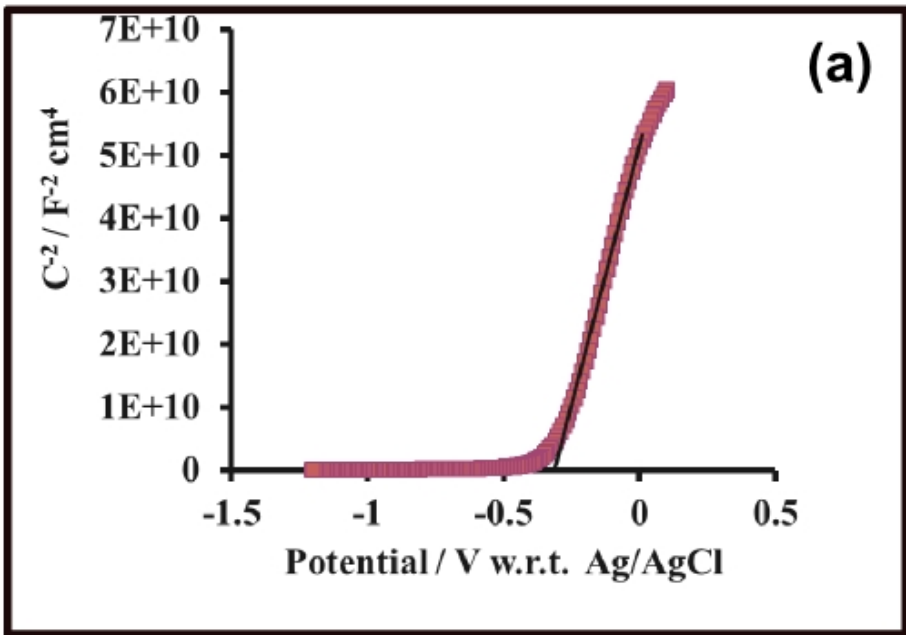
(a)
7E+10
6E+10
5E+10
4E+10
3E+10
2E+10
1E+10
0
C-2 / F-2 cm4
-1.5
-1
-0.5
0
0.5
Potential / V w.r.t. Ag/AgCl

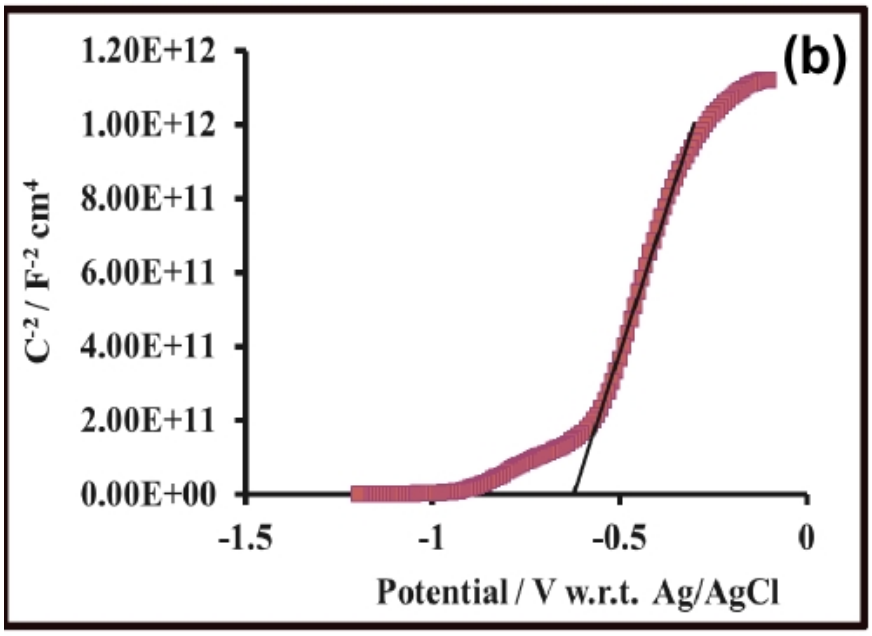
(b)
1.20E+12
1.00E+12
8.00E+11
6.00E+11
4.00E+11
2.00E+11
0.00E+00
C-2 / F-2 cm4
-1.5
-1
-0.5
0
Potential / V w.r.t. Ag/AgCl

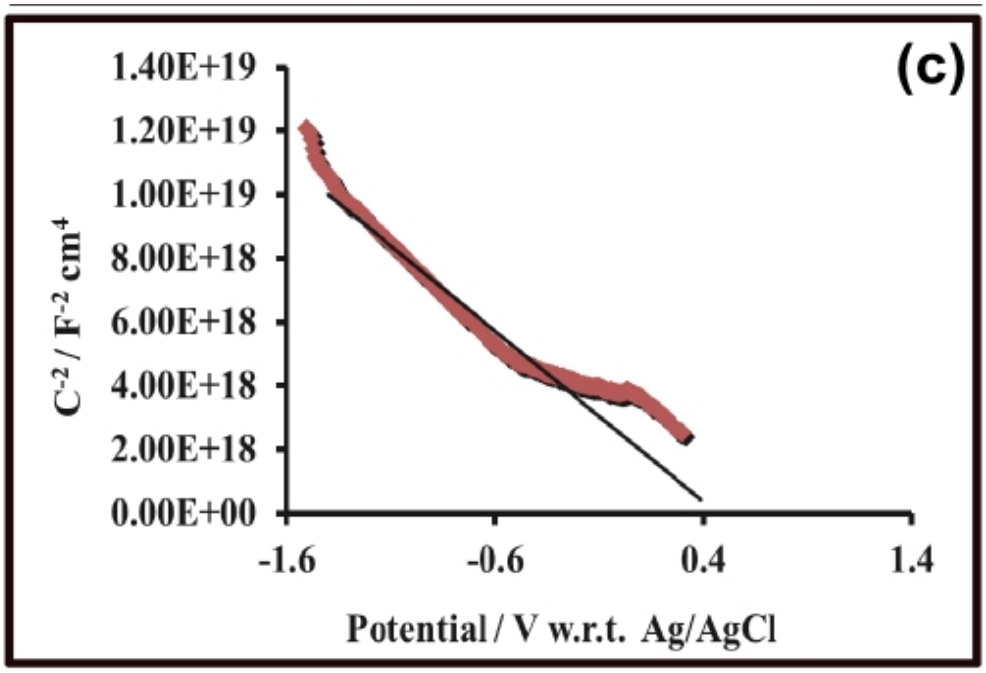

Fig. S8. (a), (b) and (c) are the Mott Schottky plots for FANTs, LANTs, and HANTs, respectively, where *n*-type semiconducting character is observed for FANTs and LANTs while *p*-type character is observed for HANTs.

Table. 1. Properties of FANTs, HANTs and LANTs

Properties	**FANT**	**HANT**	**LANT**
Shape	Square	Square	Circular
Average nanotube dimensions	Wall spacing of 50 nm; wall thickness of 15 nm	Wall spacing of 50 nm; wall thickness of 20 nm	Diameter of 50 nm; wall thickness of 10 nm
Crystal phase	Rutile	Rutile	Anatase
Type of conduction	*n*-type	*p*-type	*n*-type
Carrier concentration [cm^{-3}]	1.5×10^{18}	2.8×10^{12}	7.0×10^{19}
Charge transport resistance*	10^3 Ω	10^6 Ω	10^3 Ω

*These are approximate values, and their variation with potential is given in **Fig. S7.** (f)

REFERENCES

1. Yahia, S. A. A.; Hamadou, L.; Kadri, A.; Benbrahim, N.; Sutter, E. M. M., Effect of Anodizing Potential on the Formation and EIS Characteristics of TiO2 Nanotube Arrays. *J Electrochem Soc* **2012,** *159* (4), K83-K92;
2. Munoz, A. G., Semiconducting properties of self-organized TiO2 nanotubes. *Electrochim Acta* **2007,** *52* (12), 4167-4176;
3. Munoz, A. G.; Chen, Q.; Schmuki, P., Interfacial properties of self-organized TiO2 nanotubes studied by impedance spectroscopy. *J Solid State Electr* **2007,** *11* (8), 1077-1084.